p-[^{123}I]iodo-L-phenylalanine for detection of pancreatic cancer: basic investigations of the uptake characteristics in primary human pancreatic tumour cells and evaluation in in vivo models of human pancreatic adenocarcinoma

Samuel Samnick[1], Bernd F. M. Romeike[2], Boris Kubuschok[3], Dirk Hellwig[1], Michaela Amon[4], Wolfgang Feiden[2], Michael D. Menger[4], Carl-Martin Kirsch[1]

[1] Department of Nuclear Medicine, Saarland University Medical Center, Homburg/Saar, Germany
[2] Department of Neuropathology, Saarland University Medical Center, Homburg/Saar, Germany
[3] Department of Internal Medicine I, Saarland University Medical Center, Homburg/Saar, Germany
[4] Department of Clinical Experimental Surgery, Saarland University Medical Center, Homburg/Saar, Germany

Received: 12 October 2003 / Accepted: 9 December 2003 / Published online: 14 January 2004

Abstract. Pancreatic cancer is associated with the worst 5-year survival rate of any human cancer. This high mortality is due, in part, to difficulties in establishing early and accurate diagnosis. Because most tumours share the ability to accumulate amino acids more effectively than normal tissues and any other pathology, assessment of amino acid transport in tumour cells using radiolabelled amino acids has become one of the most promising tools for tumour imaging. This study investigated the potential of *p*-[^{123}I]iodo-L-phenylalanine (IPA) for detection of pancreatic cancer by single-photon emission tomography. IPA affinity for pancreatic tumour was investigated in human pancreatic adenocarcinoma PaCa44 and PanC1 cells, followed by analysis of the underlying mechanisms of tracer accumulation in neoplastic cells. Thereafter, IPA was evaluated for targeting of pancreatic tumours using SCID mice engrafted with primary human pancreatic adenocarcinoma cells, as well as in acute inflammation models in immunocompetent mice and rats. IPA accumulated intensively in human pancreatic tumour cells. Radioactivity accumulation in tumour cells following a 30-min incubation at 37°C/pH 7.4 varied from 41% to 58% of the total loaded activity per 10^6 cells. The cellular uptake was temperature and pH dependent and predominantly mediated by specific carriers for neutral amino acids, namely the sodium-independent and L-leucine-preferring (L-system) transporter and the alanine-, serine- and cysteine-preferring (ASC-system) transporter. Protein incorporation was less than 8%. Biodistribution studies showed rapid localization of the tracer to tumours, reaching 10%±2.5% to 15%±3% of the injected dose per gram (I.D./g) in heterotopic tumours compared with 17%±3.5% to 22%±4.3% I.D./g in the orthotopic tumours, at 60 and 240 min post injection of IPA, respectively. In contrast, IPA uptake in the gastrointestinal tract and areas of inflammation remained moderate and decreased with time. Excellent tumour detection was obtained by gamma camera imaging. The specific and high-level targeting of IPA to tumour and the negligible uptake in the gastrointestinal tract and areas of inflammation indicate that *p*-[^{123}I]iodo-L-phenylalanine is a promising tracer for differential diagnosis of pancreatic cancer.

Keywords: Pancreatic cancer – SCID mouse model – Differential diagnosis – Amino acids – SPET imaging

Eur J Nucl Med Mol Imaging (2004) 31:532–541
DOI 10.1007/s00259-003-1445-1

Samuel Samnick (✉)
Department of Nuclear Medicine,
Saarland University Medical Center,
66421 Homburg/Saar, Germany
e-mail: rassam@uniklinik-saarland.de
Tel.: +49-6841-1622201, Fax: +49-6841-1624692

Introduction

Of all the gastrointestinal tumours, pancreatic cancer has one of the worst prognoses. This high mortality rate results from difficulty in early detection, the lack of effective treatment and limited knowledge of the biological characteristic of the disease [1, 2]. At present, only radical resection of the tumour with the surrounding lymph nodes provides a chance of cure. Unfortunately, this option is limited to only 10–20% of patients because the majority of cases are diagnosed at late stages of disease

[3, 4, 5]. At the time of diagnosis, the tumour is often already large, with invasion of surrounding tissue or metastasis to distant organs. Therefore, beside substantial attempts to improve our understanding of the malignancy, major efforts have to be directed towards earlier and more accurate diagnosis of the disease with a view to improving the outcome in patients with pancreatic cancer.

Development of novel diagnostic modalities requires appropriate models that closely mimic the clinical course of the disease in humans. A suitable in vivo model for studying pancreatic carcinomas is the severe combined immunodeficient (SCID) mouse. The unique feature of this model is that the implanted human tissues maintain their normal architecture and function [6, 7]. In particular, primary human pancreatic cancers engrafted into SCID mice disseminate in a pattern analogous to human disease [8]. On the other hand, because there is no highly sensitive clinical test for the diagnosis of pancreatic cancer, intensive efforts have been made to explore imaging methods for the detection and staging of pancreatic carcinomas. However, the detection of pancreatic tumours by current imaging techniques, and especially accurate differentiation between inflammatory, i.e. acute or chronic pancreatitis, and neoplastic masses, remains problematic [9, 10, 11]. One promising approach that appears more sensitive and accurate than other imaging modalities, including computer tomography, magnetic resonance imaging (MRI), ultrasonography and positron emission tomography (PET) with fluorine-18 labelled deoxyglucose, is the use of tumour-affine radiolabelled amino acids to study physiological processes associated with the high utilization of amino acids in malignant cells non-invasively [12, 13]. Previous investigations have demonstrated that tumour imaging with amino acid tracers is less influenced by inflammation due to the generally low accumulation of amino acids in inflammatory cells [13, 14, 15, 16]. This indicates that amino acid tracers with high affinity for pancreatic cancer are potentially more tumour specific and therefore more suitable for differentiating between viable neoplastic tissues and inflammatory lesions. However, development of amino acid-based tracers for pancreatic tumour diagnosis has not been the subject of intensive study in the past decade. As part of our efforts to explore radiolabelled amino acids for non-invasive diagnosis of pancreatic cancer, we developed a series of tumour-affine radioiodinated amino acids. Among them, iodine-123 labelled L-phenylalanine, *p*-[^{123}I]iodo-L-phenylalanine (IPA), showed marked affinity for pancreatic tumours in a previous in vitro experiment [17, 18].

In this report, we studied the uptake characteristics of IPA in cultured human pancreatic adenocarcinoma cells, followed by investigation of the mechanisms promoting cellular uptake. Thereafter, IPA was evaluated in an orthotopic and heterotopic model of human pancreatic cancer in SCID mice, as well as in inflammation models in immunocompetent mice and rats, in order to assess its potential as a tracer for accurate targeting of pancreatic tumours by means of routine single-photon emission tomography (SPET).

Materials and methods

Reagents. Sodium [^{123}I]iodide for radiolabelling and [^{18}F]fluorodeoxyglucose (FDG) were commercially obtained from Forschungszentrum Karlsruhe (Karlsruhe, Germany). L-Alanine, L-phenylalanine, L-tyrosine, L-leucine, L-serine, L-cysteine, L-leucine and their D-isomers, as well as 2-amino-2-norbornane-carboxylic acid (BCH), α-(methylamino)-isobutyric acid (MeAIB), nigericin, valinomycin, 4-bromo-L-phenylalanine and non-radiolabelled 4-iodo-L-phenylalanine ("cold" IPA) were from Sigma-Aldrich (Deisenhofen, Germany). Concanavalin A (ConA) for induction of acute inflammation was purchased from ICN (Eschwede, Germany). ConA was dissolved in PBS (pH=7) for injection. Unless otherwise stated, all other solvents were of analytical or clinical grade and were either obtained from Merck (Darmstadt, Germany) or purchased via the local university hospital pharmacy. Radioactivity in tissues, blood and tumour was measured on a Berthold LB 951 G scintillation counter (Berthold, Wildbad, Germany) after reference samples (triplicates) of the injected dose had been prepared as standards.

Preparation of p-[123I]iodo-l-phenylalanine. IPA was prepared by non-isotopic Cu(II)-assisted [^{123}I]iodo-debromination of *p*-bromo-L-phenylalanine in the presence of ascorbic acid. IPA was isolated from unreacted starting materials and radioactive impurities by isocratic reverse-phase HPLC and the fraction containing the radiopharmaceutical was collected into a sterile tube, buffered with PBS (pH 7.4) and sterile-filtered through a 0.22-µm filter into an evacuated sterile tube prior to studies. Details concerning the radiosynthesis and formulation have been described previously [17, 19].

Cell cultures. The human pancreatic adenocarcinoma PaCa44 (established by Dr. M. v. Bülow, Mainz, Germany) and PanC-1 (American Type Culture Collection, Rockville, MD) cell lines were provided by the oncological research laboratory of the University Center of Saarland (Homburg, Germany). Cells were cultivated in RPMI-1640 medium containing 10% (v/v) heat-inactivated fetal calf serum (FCS), penicillin (50 U/ml), streptomycin (50 µg/ml) and 50 µl insulin (10 µl/ml) (PromoCell, Heidelberg, Germany). The cells were incubated in a humidified 5% CO_2 incubator at 37°C. Cells were passaged routinely every 5 days. Before the experiment, subconfluent cell cultures were trypsinized with a solution of 0.05% trypsin in PBS without Ca^{2+} and Mg^{2+} and containing 0.02% EDTA. Cells were washed with medium and placed in PBS shortly before implantation or uptake experiments after counting by vital staining on a haemocytometer. Cells were free of mycoplasmas. Viability of the cells was assessed by trypan blue and was >95%.

Cell uptake experiments. To assess non-specific binding of the tracer to plastic tubes, they were presaturated with 1% bovine serum albumin in 0.1 *M* PBS (pH 7.4) followed by addition of freshly prepared IPA. The solution was maintained in an incubator at 37°C for 30–180 min, followed by treatment with ice-cold PBS at the end of the experiment. The radioactivity binding to plastic tubes was less than 0.5% of total loaded radioactivity for incubation periods up to 180 min.

All experiments were performed fourfold, simultaneously with 250,000, 500,000 and 10^6 freshly resuspended human pancreatic tumour cells. Before the experiments, subconfluent cells were trypsinized as described above. The suspension was mixed thoroughly, and transferred to a 50-ml centrifuge tube (Falcon, Becton Dickinson, USA). Cells were centrifuged for 5 min at 200×*g*; the resulting supernatant was removed and the pellet resuspended in serum-free Dulbecco's modified Eagle medium and then transferred to Eppendorf tubes at concentrations of 10^6 cells/ml for the uptake investigations. Before the incubation with IPA, the pancreatic tumour cells were pre-incubated for 15 min in 500 µl medium at 37°C in 1.5-ml Eppendorf centrifuge tubes. Aliquots of 30–50 µl (10^6–1.5×10^6 cpm) freshly prepared IPA were added and cells were incubated at 37°C for 1, 2, 5, 15, 30, 60, 90 and 120 min while shaking. Uptake was stopped with 500 µl ice-cold PBS (pH 7.4) and an additional 3-min in an ice bath. The cells were then centrifuged for 2 min at 300×*g*, the supernatant removed and the pellet washed three times with ice-cold PBS. Cell pellets were counted for radioactivity together with three aliquots of standards on a Berthold LB951 gamma counter. The percentage of binding of IPA was calculated by the formula: (cpm cell pellet/mean cpm radioactive standards)×100. The results were expressed either as percent of the applied dose per 10^6 cells or as cpm/1,000 cells for better comparison.

In separate experiments the uptake of IPA into pancreatic tumour cells was investigated at different temperatures (4, 20 and 37°C, pH 7.4) and pH (5.0–9.0, 37°C), as well as in sodium-containing and in high K^+ medium (135 mm KCl). Furthermore, the contribution of the mitochondria to the cellular uptake was assessed in the presence of valinomycin and nigericin (1 mmol/l, 100 µl), which are known to disrupt the metabolism of mitochondria. Radioactivity retained in tumour cells was determined as described above after a 30-min incubation at 37°C/pH 7.4.

Determination of the protein-incorporated fraction. The fraction of IPA incorporated into protein was determined by acid precipitation. After a 30-min incubation of the samples (10^6 tumour cells) with IPA at 37°C, the medium was removed and the cells washed as described above. The cells were detached with 250 µl PBS containing 1% EDTA, followed by addition of 250 µl 10% trichloroacetic acid. After an additional 30 min at 0°C while shaking, samples were centrifuged at 10,000×*g* for 5 min. The supernatant was removed, and the pellet washed three times with ice-cold PBS. Radioactivity in the acid-precipitable fraction was counted as described above.

Determination of the mechanisms underlying the tracer uptake into tumour cells. Competitive inhibition experiments were carried out to characterize the mechanisms promoting the uptake of IPA into human pancreatic carcinoma cells. For this purpose, suspensions containing 10^6 tumour cells/ml were pre-incubated with 100 µl of specific inhibitors for amino acid transport and with selected neutral L- and D-amino acids with a known carrier system. Aliquots of 30–50 µl (10^6–1.5×10^6 cpm) freshly prepared IPA were added, followed by incubation of the mixture at 37°C/pH 7.4 for 30 min. At the end of the incubation, 0.5 ml ice-cold PBS (pH 7.4) was added to stop the reaction. Cell pellets were isolated after centrifugation and radioactivity retained in tumour cells determined on a gamma counter as described above.

The following specific amino acid carrier inhibitors and neutral amino acids were used: BCH, MeAIB and alanine-serine-cysteine (1:1:1), L-leucine, L-phenylalanine, L-tyrosine, L-proline, D-phenylalanine, D-tyrosine and D-proline. The concentration of the inhibitors used was 1 and 5 mmol/l. A parallel experiment was performed with increasing concentrations of unlabelled 4-iodo-L-phenylalanine to assess the capacity of the transport system.

Animals. All animal experiments were conducted in accordance with the Guide for the Care and Use of Laboratory Animals published by the US National Institutes of Health (NIH Publication No. 85-23, revised 1996) and in compliance with the German animal protection law. Experiments were approved by the local district government (Saarpfalz-Kreis, AZ: K 110/180-07, January 22, 2002).

Pathogen-free severe combined immunodeficient (SCID) mice (age: 7–8 weeks; strain: CB-17-scid/IcrCrl of both sexes) were obtained from Charles River Germany (Sulzfeld, Germany). They were maintained under sterile conditions in the animal facility of the Saarland University Medical Center at the Institute of Clinical and Experimental Surgery. After a period of adaptation, implantations were performed in SCID mice, which were 8–10 weeks old at the time of cell inoculation. In addition, immunocompetent CD rats (230–300 g) and ICR mice (25–32 g) (Charles River, Sulzfeld, Germany) were used to induce acute inflammation, because SCID mice lack the ability to develop inflammation after ConA inoculation, as confirmed in a control experiment.

Tumour implantation and induction of inflammation. Two different tumour implantation methods were used in this study: heterotopic implantation by subcutaneous injection of primary human pancreatic tumour cells into the flank of SCID mice and orthotopic inoculation of tumour cells into the pancreas of the animals.

A first group of mice (n=36) received subcutaneous injections, into the right flank, of 2.0–2.5×10^6 human pancreatic adenocarcinoma PaCa44 or PanC-1 cells in 35–60 µl PBS. For the orthotopic implantation, animals (n=36) were anaesthetized by intraperitoneal administration of a mixture of ketamine (70 mg/kg) and xylazine (Rompun 2%, 20 mg/kg). Thereafter, laparotomy was performed by a midline incision, and the spleen and distal pancreas were mobilized. Then, 1.5–2.0×10^6 tumour cells in a volume of 20–25 µl PBS were injected into the proximal part of the exposed pancreas. After cell inoculation, the incision was closed in two layers using continuous vicryl suture (Metric 1.5, Norderstedt, Germany). After tumour implantation, the animals were inspected daily for complications and checked for tumour formation visually and by palpation. Tumour size was calculated by the following formula: tumour volume (cm^3)=$W^2\times L\times1/2$; where L is the length (cm) and W the width (cm) of the tumour [20]. Tumour growth was additionally monitored non-invasively by MRI, starting 10 days after implantation.

Inflammation was induced by injection of a solution of ConA (150 µg in 100 µl PBS) into the right posterior foot pad of male immunocompetent rats and mice (n=15) as described elsewhere [15].

Magnetic resonance imaging. MRI was performed using a 2.4-Tesla small animal magnetic resonance tomograph (Brucker Biospec 2.4, Karlruhe, Germany). This system was equipped with a mouse coil to fix the animal and transmit homogeneous signals. All SCID mice were imaged while under ketamine/xylazine anaesthesia. Multiple axial and coronal images (T1 and T2 weighted) were acquired for 20 min without contrast media. The parameters used were: T1 weighted: TR=100 ms, TE=6.5 ms, flip angle 30°, FOV=2×2 cm, 256×128×64 matrix; T2 weighted: TR=500 ms, TE=17.5 ms, 1 acquisition, RARE factor 16, FOV=2×2 cm, 256×256×32 matrix, slice thickness 16 mm. The size of the detect-

ed tumours was calculated from the multislice T2-weighted images by counting the total number of tumour voxels in each tumour-containing slice and multiplying by the voxel size (0.1 mm^3), as described previously [21].

Biodistribution studies and gamma camera and PET imaging. Biodistribution studies were carried out in SCID mice 3–4 weeks after tumour implantation to assess tumour and organ uptake of IPA quantitatively. To this end, tumour-bearing mice were anaesthetized by ketamine/xylazine as described above. Thereafter, freshly prepared IPA (2–3 MBq in 0.1–0.2 ml injectable solution) was administered via a tail vein and animals held in metabolic cages. Four mice per group were sacrificed 15, 60 and 240 min after injection. The abdomen and thoracic cavity of the animals were examined systematically for the presence of tumour and metastases. Samples of blood were obtained by heart puncture. Tumours and various organs were excised and weighed. Radioactivity concentration in organs and tumours was determined by gamma counting. After correction for physical decay, percent injected dose per gram tissue (% I.D./g) was calculated for each tissue. At the end of the experiment, tumour mass and organs of interest, including the lung, kidneys, pancreas, spleen, stomach, liver, intestine and bladder, were examined histopathologically. ICR mice and rats with acute inflammations received i.v. injections of IPA (2–4 MBq) in the same manner, 24 h after ConA inoculation, while under pentobarbital (50 mg/kg, i.p.) narcosis. Four animals per time point were sacrificed at 15, 60 and 240 min after injection of the tracer. Radioactivity accumulation in organs and inflammatory lesions was determined by gamma counting as described above, followed by histopathological examinations of the tissues.

In separate experiments, whole-body distribution of the tracer in tumour-bearing SCID mice and in rats presenting acute inflammation was visualized at different time points after intravenous administration of 8–12 MBq of IPA. Images were acquired over 10 min using a single-head gamma camera [APEX SPX 4, Elscint Medical Systems (formerly Elscint Ltd), Haifa, Israel]. The camera was equipped with low-energy, high-resolution parallel-hole collimators (APC-45S, Elscint), and 20% energy window was used, centered on the 159-keV photopeak of ^{123}I. At the end of the gamma scintigraphy, rats with induced acute inflammation were subsequently injected with 10 MBq of FDG and PET imaging was performed at 60 min post injection on an ECAT ART PET scanner (Siemens/CTI, USA). Attempts to acquire the whole-body distribution of FDG in SCID mice (25–30 g) accurately by means of PET were unsuccessful owing to the low resolution of our PET scanner.

Histological examination. Tumours and tissues from experimental animals were fixed in 4% neutral buffered formalin and embedded in paraffin wax. Sections were stained with haematoxylin-eosin and Verhoeff-van Gieson and examined histopathologically.

Statistical analysis. The statistical significance of differences among experimental groups was determined by Student's *t* test. A *P* value less than 0.05 was considered significant.

Results

p-*[^{123}I]iodo-L-phenylalanine*

The *p*-[^{123}I]iodo-L-phenylalanine (IPA) used in the present study was obtained in 90%±5% radiochemical yield after HPLC isolation. A radiochemical purity of >99% was obtained. IPA was formulated as previously described [17, 19] prior to use in in vitro and in vivo experiments.

Cell uptake and determination of uptake mechanisms

The uptake kinetics of IPA into primary human pancreatic adenocarcinoma PaCa44 and PanC1 cells and the results of inhibition experiments are given in Fig. 1. IPA showed high accumulation in pancreatic tumour cells. The IPA uptake into tumour cells was rapid and linear during the first 7 min. More than 70% of the total radioactivity binding in cells, as determined over 120 min, occurred within the first 5 min of incubation. The uptake kinetics increased slowly from 15 min onwards. Radioactivity accumulation in pancreatic tumour cells following a 30-min incubation at 37°C/pH 7.4 varied from 41% to 58% of the total loaded activity per 10^6 cells (490–610 and 570–820 cpm/1,000 cells for PaCa44 and PanC1, respectively). Pre-incubation of tumour cells with different amount of unlabelled 4-iodo-L-phenylalanine ("cold IPA") resulted in no significant reduction in the tracer uptake up to a concentration of 50 µmol/l (Fig. 1B). In addition, the tracer uptake was only slightly tumour cell concentration dependent between 250,000 and 10^6 cells (data not shown). Compared with the uptake at 37°C, that at 4°C was reduced by up to 93%±5% (P<0.01). Cell precipitation with trichloroacetic acid after incubation with IPA for 30 min demonstrated that IPA incorporation into protein is relatively low, at 7%±3% of the radioactivity in the acid-precipitable fraction . While lowering the medium pH (from 7.4 to 5.0) resulted in a reduction in the cellular uptake by 40%±10%, neither depolarizing the membrane potential in high K^+ buffer nor increasing the sodium concentration affected the accumulation of IPA in tumour cells significantly <25% (Fig. 1C). Valinomycin and nigericin, which are known to influence the cellular mitochondrial activity, induced a slight alteration in the cellular uptake of the tracer, suggesting that membrane and mitochondrial potentials play a minor role in the cellular uptake. In contrast, preloading pancreatic tumour cells with BCH and L-alanine-serine-cysteine, or with the neutral L-amino acids L-leucine, L-alanine, L-phenylalanine and L-tyrosine, affected the uptake of IPA by up to 95%±3%, (P<0.01). In contrast, MeAIB, the selective inhibitor of the amino acid transport system A, L-proline and neutral D-amino acids induced no significant alteration in the uptake of the amino acid tracer into human pancreatic tumour cells.

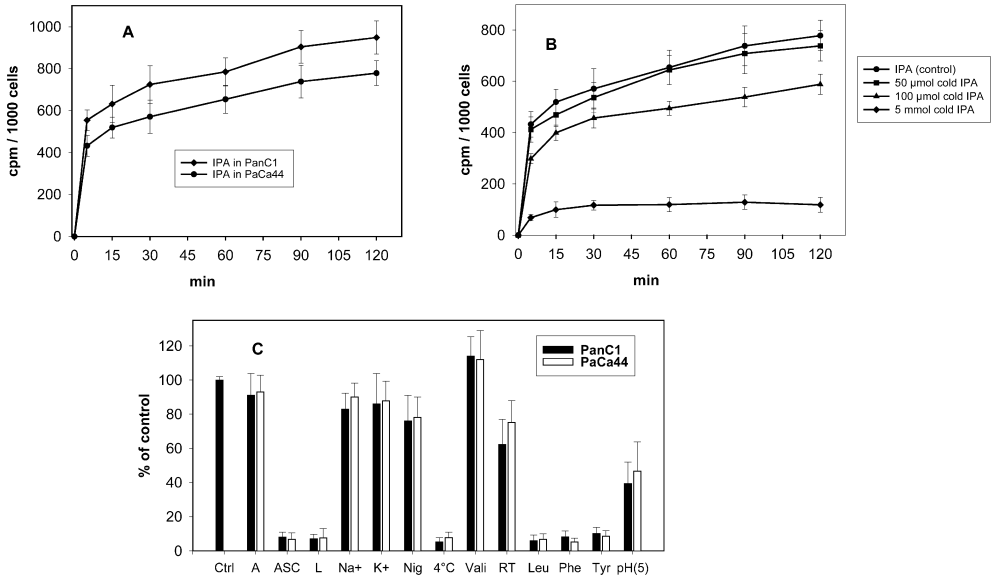

Fig. 1A–C. Uptake kinetics of IPA in primary human pancreatic adenocarcinoma PaCa44 and PanC1 cells at 37°C (pH 7.4) (**A**), and after pre-incubation of tumour cells (PaCa44) with unlabelled "cold" IPA (50 µmol, 100 µmol and 5 mmol) for 15 min (**B**). **C** Alteration of tracer accumulation by α-(methylamino)isobutyric acid (*A*), L-alanine/L-serine/L-cysteine (*ASC*), 2-amino-2-norbornane-carboxylic acid (*L*), sodium (*Na+*), KCl (*K+*), nigericin (*Nig*), valinomycin (*Vali*), room temperature (*RT*), L-leucine (*Leu*), L-phenylalanine (*Phe*) and L-tyrosine (*Tyr*) after co-incubation for 30 min, as % of control (*Ctrl*). The influence of temperature and pH on the IPA uptake into human pancreatic tumour cells is also shown (n=4, mean±SD)

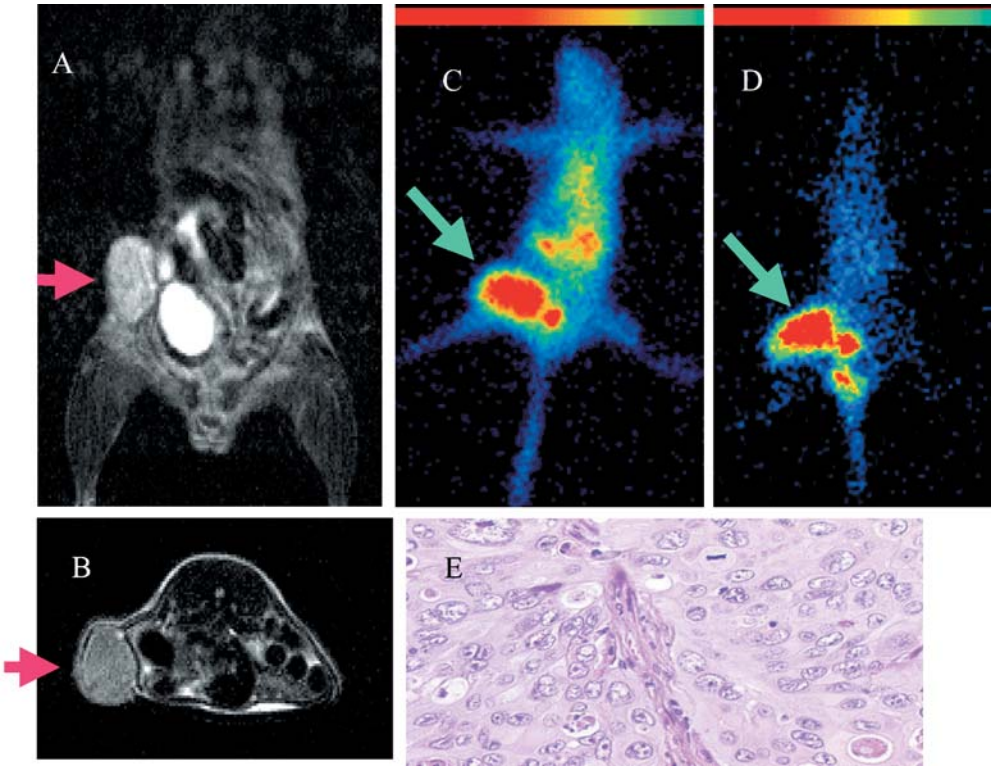

Fig. 2A–E. T2-weighted coronal (**A**) and T1-weighted axial (**B**) MRI of a heterotopic human pancreatic adenocarcinoma PaCa44 xenograft, demonstrating tumour in the flank of the SCID mouse. Corresponding whole-body gamma camera imaging at 120 min (**C**) and 18 h (**D**) after injection of IPA (10 MBq) demonstrates high and specific uptake of the tracer by tumour and renal excretion, while uptake in the gastrointestinal tract and the remaining body was qualitatively insignificant over time (**D**). Histological confirmation of tumour (magnification 200-fold) in haematoxylin and eosin (H&E) paraffin sections is shown in (**E**). *Arrows* indicate the tumour location

In vivo models and animal studies

All SCID mice developed a pancreatic tumour within 4 weeks after implantation of primary human adenocarcinoma cells. The heterotopic implanted tumours were accurately detected non-invasively by MRI and confirmed histologically (n=36, tumour=100%). The heterotopic PaCa44 tumours were palpable 14–18 days after subcu-

taneous cell inoculation. In comparison, accurate detection of the heterotopic PanC1 tumours by palpation was possible from 3 weeks onwards. Tumour size, as calculated by the method described by Adachi et al. [20] was 0.75±0.35 cm^3 by 3.5–4 weeks after subcutaneous injection of tumour cells, compared with 0.62±0.27 cm^3 by MRI determination. Figure 2 shows an example of T1-weighted coronal (Fig. 2A) and axial (Fig. 2B) MR images of a heterotopic PaCa44 tumour xenograft. The corresponding whole-body scintigraphic images obtained with a gamma camera at 120 min (Fig. 2C) and 18 h (Fig. 2D) after injection of IPA demonstrate specific uptake of the amino acid tracer in tumour tissues and excellent visualization of the tumour masses. Histological confirmation of the tumour after autopsy is demonstrated in Fig. 2E. A representative example of T1-weighted MRI of an orthotopic tumour xenograft and the corresponding gamma camera image, as well as the histological analysis of the isolated pancreas, are shown in Fig. 3. MRI was true positive in only 70% and 90% of the histologically confirmed orthotopic PanC1 and PaCa44 tumours, respectively. Most of the orthotopic xenotransplanted tumours could not be confirmed by palpation. The size of tumours, as determined by MRI at 4 weeks after cell inoculation into the pancreas, ranged from 0.230 to 0.675 cm^3.

The heterotopic xenotransplanted tumours showed only local invasion of adjacent muscle. No distant metastases were macroscopically or histologically determined in the abdomen or thoracic cavity even 4 weeks after subcutaneous implantation of human pancreatic PaCa44 and PanC1 tumour cells. In contrast, most of the orthotopic implanted tumours grew beyond the pancreas, with invasion of adjacent organs and metastases in different abdominal sites.

Biodistribution results for IPA in human pancreatic tumour-bearing SCID mice are summarized in Fig. 4. IPA showed high accumulation in engrafted tumours following intravenous administration. Tumour uptake increased gradually with time, while accumulation in muscle, spleen, kidney, stomach, pancreas, intestine and liver remained moderate and decreased over time. Comparison of the two implantation models showed that the uptake of IPA by the heterotopic tumours was lower than that by the orthotopic tumours (P<0.02). At 60 and 240 min post injection of IPA, radioactivity binding in tumour amounted to, respectively 10%±2.5% and 15%±3% of the injected dose per gram tumour (I.D./g) in heterotopic tumours (Fig. 4A, B) compared with 17%±3.5% and 22%±4.3% I.D./g in orthotopic tumours (Fig. 4C, D). The corresponding mean tumour-to-organ ratios for heterotopic and orthotopic tumours at 60 and 240 min were 2.2±0.7 and 6.4±1.6 (tumour/blood), 3.4±1.1 and 6.7±1.5 (tumour/spleen), 2.1±0.7 and 4.4±1.6 (tumour/pancreas), 3.8±1.1 and 7.6±1.3 (tumour/intestine), 3.4±1.3 and 7.2±1.5 (tumour/liver), and 6.1±1.4 and 11.5±1.6 (tumour/muscle), respectively.

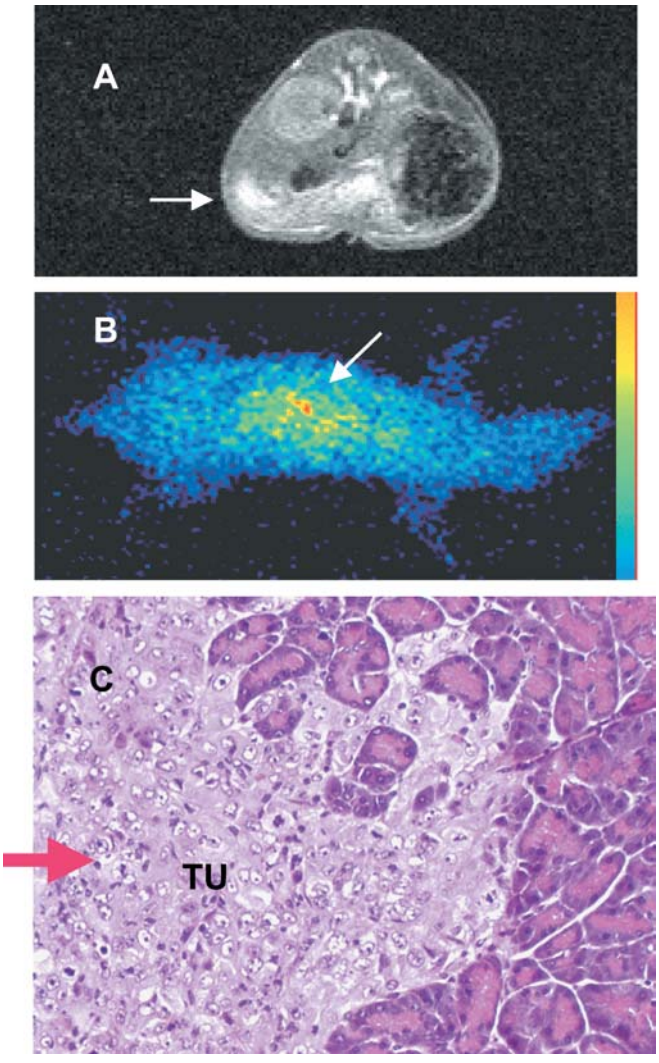

Fig. 3A–C. Axial T1-weighted MRI (**A**) of an orthotopic human pancreatic PanC1 xenograft and the corresponding gamma camera image (**B**) of the SCID mouse 360 min after administration of IPA (8 MBq) through the tail vein. Tumour showed invasion into liver and intestine as well as metastases in the abdomen. Histological analysis of the isolated pancreas (200-fold; H&E paraffin sections) confirmed the formation of a poorly differentiated adenocarcinoma (*TU*) within the pancreas (**C**). *Arrows* indicate the tumour location

Data on the biodistribution of IPA in the inflammation model in immunocompetent mice are presented in Table 1. At 15, 60 and 240 min, the radioactivity accumulation in areas of ConA-induced inflammation was 2.5%±1.2%, 2.4%±1.1% and 1.9%±0.7% I.D./g, respectively, versus 1.8%±0.5%, 1.9%±0.6% and 1.5%±0.8% I.D./g in the opposite left foot of the mouse, which served as a control (Table 1). The resulting ratio between uptake of IPA in areas of acute inflammation and that in the healthy skeletal muscle of immunocompetent mice was 1.1–1.3. The difference between the radioactivity accumulation in areas of

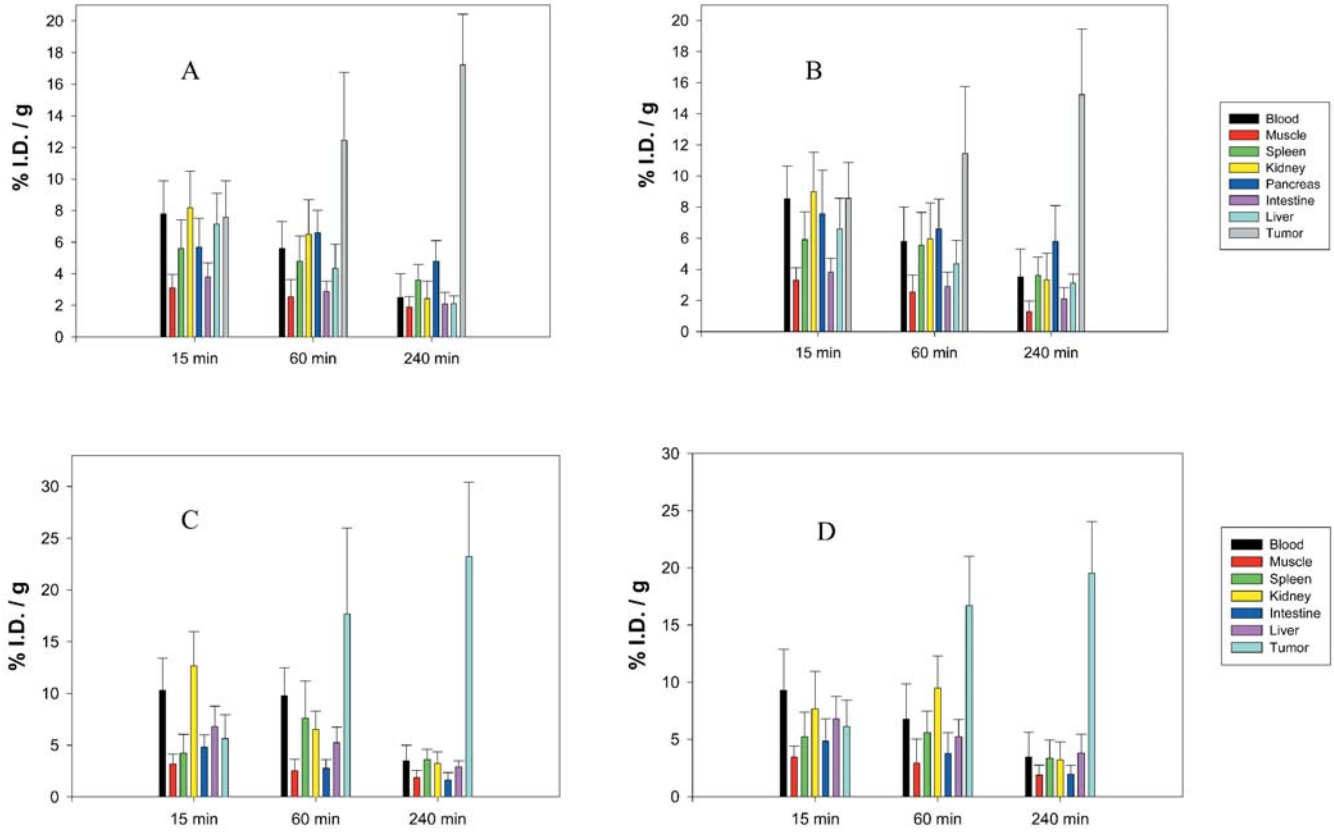

Fig. 4A–D. Tissue distribution of IPA in heterotopic (**A, B**) and orthotopic (**C, D**) human pancreatic carcinoma PaCa44 (**A** and **C**) and PanC1 (**B** and **D**)-bearing SCID mice at 15, 60 and 240 min after intravenous injection of 2–4 MBq of the tracer. Uptake is expressed as percent of injected dose/g tissue (% I.D./g), (median, *n*=4)

Table 1. Biodistribution of IPA in immunocompetent mice with ConA induced inflammation

Organ	IPA		
	15 min	60 min	240 min
Blood	4.42±0.61	2.23±0.31	1.97±0.25
Lung	1.21±0.10	1.19±0.02	0.64±0.20
Heart	1.10±0.24	0.97±0.10	0.73±0.13
Spleen	1.57±0.43	1.85±0.42	0.96±0.25
Liver	3.26±0.63	2.68±0.20	1.98±0.74
Intestine	1.45±0.53	1.94±0.23	1.04±0.18
Kidney	2.37±0.51	3.72±0.31	1.14±0.11
Pancreas	4.67±1.0	4.51±0.82	3.21±0.61
Bone	0.76±0.20	0.88±0.10	0.76±0.03
Skeletal muscle[a]	1.82±0.51*	1.93±0.63*	1.46±0.76*
Inflammatory tissue[b]	2.46±1.20*	2.41±1.12*	1.90±0.73*
Brain	0.32±0.06	0.33±0.04	0.29±0.06

Uptake is expressed in percent of injected dose/g tissue (% I.D./g), (median, *n*=4)
[a] Skeletal muscle of the opposite left foot (as control)
[b] Tissue from the area of acute inflammation
*$P>0.1$; the difference is statistically non-significant

ConA-induced inflammation and that in the opposite left foot of the mouse was not statistically significant ($P>0.1$) (Table 1). Gamma camera imaging of a rat presenting acute inflammation at 60 min after injection of IPA and the PET images of the same rat following FDG administration are shown in Fig. 5. The FDG uptake was significantly increased in areas of acute inflammation (>500%). The ratio between the uptake of FDG in inflammatory lesions and that in the healthy opposite left thigh was at least 5:1 (*n*=4). In comparison, gamma camera imaging demonstrated that the increase in IPA in inflammation was relatively moderate, at 20–25%. Histological analysis of the inflammatory lesions demonstrated the presence of lympho-histiocytic cells and

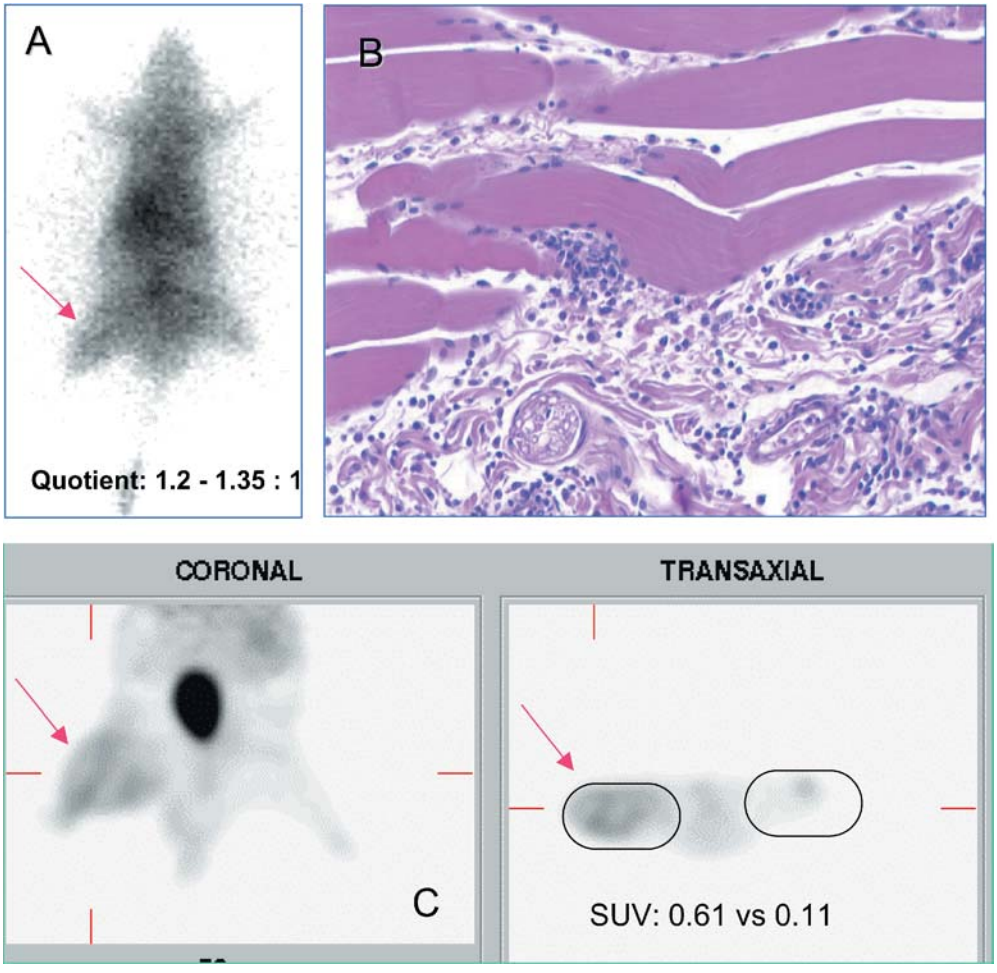

Fig. 5 A. Representative whole-body image of an immunocompetent rat bearing ConA-induced inflammation in the right foot, 60 min after i.v. injection of IPA, showing qualitatively no significant differences between the uptake of the amino acid tracer in areas of inflammation and in the unaffected left foot, used as a control. **B** Histomorphological analysis of the corresponding skeletal muscle demonstrated acute inflammatory changes mainly composed of lympho-histiocytic cells and scattered plasma cells as well as granulocytes and macrophages. H&E, original magnification ×200. **C** In comparison, the subsequent FDG-PET images of the same animal 60 min after injection of FDG shows high FDG accumulation in areas of inflammation. *Arrows* indicate the location of inflammation

scattered plasma cells, as well as granulocytes and macrophages (Fig. 5B).

Discussion

Because there is no highly sensitive clinical test for the diagnosis of pancreatic cancer, intensive efforts have been undertaken to improve both the sensitivity and the specificity of imaging techniques for the detection and staging of pancreatic carcinomas. However, although the detection of pancreatic tumours has been considerably improved using current imaging techniques, including computer tomography, ultrasonography, MRI and FDG PET, differential diagnosis of pancreatic cancers remains a challenge, especially in the early stage of disease [9, 11, 22, 23, 24]. The aim of this study was to assess experimentally the ability of the novel amino acid tracer *p*-[^{123}I]iodo-L-phenylalanine (IPA) to detect pancreatic carcinomas. IPA was found to exhibit high uptake in human pancreatic tumour cells with a continuous increase over the investigation time of 120 min. This result provides evidence of the high affinity of IPA for pancreatic tumours.

One of the major points of discussion is the underlying mechanism of tumour uptake. It is assumed that amino acid transport may be more important for tumour imaging than the incorporation of the amino acid tracer into proteins [12, 25, 26]. Therefore, we investigated the transport mechanism responsible for the uptake of IPA into pancreatic tumour cells. Several studies have characterized a number of distinct systems for the transport of amino acids inside mammalian cells [27, 28]. It has been demonstrated that the uptake of neutral amino acids into mammalian cells occurs predominantly through the A, L and ASC carrier-mediated systems [27, 29, 30]. Analogous to these experiments, we studied the cellular uptake of IPA by competitive inhibition, using substrates known to be specific inhibitors for transport-mediated systems A, L and ASC. We found that the IPA uptake into human pancreatic tumour cells was predominantly mediated by the L and ASC transport pathways. This finding was additionally confirmed by the strong inhibition of the tracer uptake by neutral L-amino acids known to be solely transported by L- and ASC-systems [28, 31]. In contrast, neutral D-amino acids did not affect the IPA uptake into cells, indicating the stereospecificity of the tracer uptake into pancreatic tumour cells. This result

is in agreement with the moderated accumulation of *p*-[^{123}I]iodo-D-phenylalanine in glioma cells observed in our previous investigations (unpublished data). Importantly, the protein incorporation of IPA was less than 8% in our study. Therefore, the high uptake of IPA into pancreatic tumour cells could be primarily associated with the increased amino acid transport activity in tumour cells. Importantly, the transport capacity for unlabelled IPA in tumour cells did not show saturation up to 200 μmol/l, confirming the relatively high capacity of the transport system.

The second goal of this study was to evaluate the ability of IPA to identify pancreatic carcinomas in vivo, and thereby to assess its potential as a tracer for accurate diagnosis of pancreatic cancer by means of SPET. We used SCID mice engrafted with primary human pancreatic adenocarcinoma cells as an animal model. MRI, autopsy and histopathological analysis demonstrated that primary human pancreatic carcinomas engrafted into SCID mice disseminated in a pattern analogous to human disease, including invasion by the tumour into adjacent organs and formation of metastases in different sites of the abdomen. Thus, our model fulfils the major requirements as an in vivo model of human pancreatic cancer and can be used for preclinical evaluations. IPA was found to accumulate intensively in implanted pancreatic tumours. This result is in agreement with data obtained in in vitro experiments. Importantly, the tracer uptake by the lung, liver, kidney, liver, stomach and intestine remained moderate and diminished considerably with time, resulting in an excellent contrast between tumour and organs, especially from 120 min onwards. The ability of SPET with IPA to detect pancreatic cancer was impressively confirmed by gamma camera imaging (Fig. 2). From 360 min onwards only tumour tissues were demonstrated scintigraphically, indicating that IPA is a highly selective tracer for non-invasive diagnosis of pancreatic tumour.

As yet, accurate clinical differentiation between inflammation and neoplastic tissues is not possible. Consequently, we also examined the uptake of IPA in areas of inflammation in comparison with the uptake by normal tissue and tumour. Inflammation was induced by inoculation of ConA into the right foot of immunocompetent rats and mice. The most prominent inflammatory reactions occurred 12–24 h after ConA injection, which is in agreement with previous reports [15]. Accumulation of IPA in areas of inflammation was moderate and comparable with the tracer uptake by the unaffected skeletal muscle of immunocompetent animals, and significantly lower than that in tumours ($P<0.01$). In comparison, the uptake of FDG increased by up to 700% in inflammatory lesions. This important finding indicates that IPA is a valuable tracer for differentiation between neoplastic masses and inflammation in vivo.

In conclusion, the radioiodinated amino acid IPA inhibits high affinity for human pancreatic cancer. Its marked accumulation in tumour reflects the increased amino acid transport activity in neoplastic cells and is predominantly mediated by the L and ASC carrier pathways. In addition to its high tumour accumulation, the uptake of IPA into the gastrointestinal tract and areas of inflammation is moderate or decreases rapidly with time, resulting in sufficiently high tumour-to-background contrast for clinical applications with SPET. These data indicate that IPA is a very promising tracer for non-invasive imaging of pancreatic carcinomas by routine SPET.

Acknowledgement. The authors express their deep appreciation to Miss Elisabeth Gluding for her assistance and expertise in animal care, Mrs. Claudia Schormann for cell cultures and Mrs. D. Wagner and Katja Fischer for their technical support in the performance of scans with MRI and the gamma camera.

References

1. Warshaw AW, Fernandez-del Castillo C. Pancreatic carcinoma. N Engl J Med 1992; 326:455–465.
2. Faivre J, Forman D, Esteve J, Obradovic M, Sant M. Survival of patients with primary liver cancer, pancreatic cancer and biliary tract cancer in Europe. Eur J Cancer 1998; 34:2184–2190.
3. Lillemore K. Current management of pancreatic cancer. Ann Surg 1995; 221:133–148.
4. Schafer M, Mullhaupt B, Clavien PA. Evidence-based pancreatic head resection for pancreatic cancer and chronic pancreatitis. Ann Surg 2002; 236:137–148.
5. Trümper L, Menges M, Daus H, Kohler D, Reinhard JO, Sackmann M, Moser C, Sek A, Jacobs G, Zeitz M, Pfreundschuh M. Low sensitivity of the ki-ras polymerase chain reaction for diagnosing pancreatic cancer from pancreatic juice and bile: a multicenter prospective trial. J Clin Oncol 2002; 21:4331–4337.
6. Mueller BM, Reisfeld RA. Potential of the scid mouse as a host for human tumors. Cancer Metastasis Rev 1991; 10:193–200.
7. Leblong V, Autran B, Cesbron JY. The SCID mouse mutant: definition and potential use as a model for immune and hematological disorders. Hematol Cell Ther 1997; 39:213–221.
8. Mohammad RM, Al-Katib A, Pettit GR, Vaitkevicius VK, Joshi U, Adsay V, Majumdar AP, Sarkar FH. An orthotopic model of human pancreatic cancer in severe combined immunodeficient mice: potential application for preclinical studies. Clin Cancer Res 1998; 4:887–894.
9. Nitzsche EU, Hoegerle S, Mix M, Brink I, Otte A, Moser E, Imdahl A. Non-invasive differentiation of pancreatic lesions: is analysis of FDG kinetics superior to semiquantitative uptake value analysis? Eur J Nucl Med Mol Imaging 2002; 29: 237–242.
10. Grino P, Martinez J, Grino E, Carnicer F, Alonso S, Perez-Berenguer H, Perez-Mateo M. Acute pancreatitis secondary to pancreatic neuroendocrine tumours. JOP 2003; 4:104–110.
11. Diederichs CG, Staib L, Vogel J, Glasbrenner B, Glatting G, Brambs HJ, Beger HG, Reske SN. Values and limitations of ^{18}F-fluorodeoxyglucose-positron-emission tomography with preoperative evaluation of patients with pancreatic masses. Pancreas 2000; 20:109–116.
12. Laverman P, Boerman OC, Corstens FH, Oyen WJ. Fluorinated amino acids for tumour imaging with positron emission tomography. Eur J Nucl Med Mol Imaging 2002; 29:681–690.

13. Jager PL, Vaalburg W, Pruim J, de Vries EG, Langen KJ, Piers DA. Radiolabeled amino acids: basic aspects and clinical applications in oncology. J Nucl Med 2001; 42:432–445.
14. Kubota R, Kubota K, Yamada S, Tada M, Takahashi T, Iwata R, Tamahashi N. Methionine uptake by tumor tissue: a microautoradiographic comparison with FDG. J Nucl Med 1995; 36:484–492.
15. Rau FC, Weber WA, Wester HJ, Herz M, Becker I, Kruger A, Schwaiger M, Senekowitsch-Schmidtke R. *O*-(2-[^{18}F]Fluoroethyl)-L-tyrosine (FET): a tracer for differentiation of tumour from inflammation in murine lymph nodes. Eur J Nucl Med Mol Imaging 2002; 29:1039–1046.
16. Lahoutte T, Mertens J, Caveliers V, Franken PR, Everaert H, Bossuyt A. Comparative biodistribution of iodinated amino acids in rats: selection of the optimal analog for oncologic imaging outside the brain. J Nucl Med 2003; 44:1489–1494.
17. Samnick S, Schaefer A, Siebert S, Richter S, Vollmar B, Kirsch CM. Preparation and investigation of tumor affinity, uptake kinetic and transport mechanism of iodine-123-labelled amino acid derivatives in human pancreatic carcinoma and glioblastoma cells. Nucl Med Biol 2001; 28:13–23.
18. Samnick S, Hellwig D, Gouverneur E, Romeike BF, Schneider G, Menger M, Kirsch CM. Evaluation of radioiodinated phenylalanine-analogues as radiopharmaceuticals to image pancreatic carcinomas in in-vivo models of human pancreatic tumors. Eur J Nucl Med Mol Imaging 2003; 30:S175.
19. Samnick S, Richter S, Romeike BF, Heimann A, Feiden W, Kempski O, Kirsch CM. Investigation of iodine-123-labelled amino acid derivatives for imaging cerebral gliomas: uptake in human glioma cells and evaluation in stereotactically implanted C6 glioma rats. Eur J Nucl Med 2000; 27:1543–1551.
20. Adachi T, Hinoda Y, Nishimori I, Adachi M, Imai K. Increased sensitivity of gastric cancer cells to natural killer and lymphokine-activated killer cells by antisense suppression of *N*-acetylgalactosaminyltransferase. J Immunol 1997; 159:2645–2651.
21. Schneider G, Fries P, Wagner-Jochem D, Thome D, Laurer H, Kramann B, Mautes A, Hagen T. Pathophysiological changes after traumatic brain injury: comparison of two experimental animal models by means of MRI. MAGMA 2002; 14: 233–241.
22. Obuz F, Dicle O, Coker A, Sagol O, Karademir S. Pancreatic adenocarcinoma: detection and staging with dynamic MR imaging. Eur J Radiol 2001; 38:146–150.
23. DiMagno EP, Reber HA, Tempero MA. AGA technical review on the epidemiology, diagnosis, and treatment of pancreatic ductal adenocarcinoma. American Gastroenterological Association. Gastroenterology 1999; 117:1464–1484.
24. Logsdon CD, Simeone DM, Binkley C, Arumugam T, Greenson JK, Giordano TJ, Misek DE, Hanash S. Molecular profiling of pancreatic adenocarcinoma and chronic pancreatitis identifies multiple genes differentially regulated in pancreatic cancer. Cancer Res 2003; 63: 2649–2657.
25. Langen KJ, Pauleit D, Coenen HH. 3-[^{123}I]Iodo-alpha-methyl-L-tyrosine: uptake mechanisms and clinical applications. Nucl Med Biol 2002; 29:625–631.
26. Miyagawa T, Oku T, Uehara H, Desai R, Beattie B, Tjuvajev J, Blasberg R. "Facilitated" amino acid transport is upregulated in brain tumors. J Cereb Blood Flow Metab 1998; 18: 500–509.
27. Shotwell, MA, Kilberg MS, Oxender DL. The regulation of neutral amino acid transport in mammalian cells. Biochim Biophys Acta 1983; 737:267–284.
28. Saier MH, Daniels GA, Boerner P, Lin J. Neutral amino acid transport systems in animal cells: potential targets of oncogene action and regulators of cellular growth. J Membr Biol 1988; 104:1–20.
29. Segel GB, Woodlock TJ, Murant FG, Lichtman MA. Photoinhibition of 2-amino-2-carboxybicyclo[2,2,1]heptane transport by *O*-diazoacetyl-L-serine. An initial step in identifying the L-system amino acid transporter. J Biol Chem 1989; 264: 16399–16402.
30. Barker GA, Wilkins RJ, Golding S, Ellory JC. Neutral amino acid transport in bovine articular chondrocytes. J Physiol 1999; 514:795–808.
31. Jara JR, Martinez-Liarte JH, Solano F, Penafiel R. Transport ofL-tyrosine by B16/F10 melanoma cells: the effect of intracellular content of other amino acids. J Cell Sci 1990; 97:479–485.